2014 IEEE International Conference on Robotics & Automation (ICRA)
Hong Kong Convention and Exhibition Center
May 31 - June 7, 2014. Hong Kong, China

Toward a Solution to the Snapping Problem in a Concentric-Tube Continuum Robot: Grooved Tubes with Anisotropy

Ji-Suk Kim, Dae-Young Lee, *Student Member, IEEE,* Keri Kim, Sungchul Kang, and Kyu-Jin Cho, *Member, IEEE*

***Abstract*— The concentric-tube continuum robot generates distal end motions by translating and rotating the proximal ends of pre-curved tubes that overlap concentrically. This robot does not require additional actuators along the tubes because the overall curvature and distal end position are determined solely by interactions between the inner and outer tubes. However, under certain conditions, the rotation of the distal end is hindered as the actuation energy accumulates into torsional energy of the tubes. As the distal ends are rotated further, the accumulated energy from the twisting is suddenly released, which makes the tubes snap to a remote position. This is called the snapping problem, and it considerably limits the performance of the robot. In this paper, we propose a novel design for the concentric tubes to eliminate the snapping problem. The new design creates groove patterns on superelastic nitinol tubes to make the tubes more flexible to bending than twisting. Simulations and experiments were performed to verify that the tubes with our groove patterns had anisotropic structural characteristics, and video image analysis verified that this structural property can eliminate the snapping problem. A concentric-tube robot with this new tube design can have a larger workspace area because tubes with greater curvatures can be used without the snapping problem.**

I. Introduction

Recently, there has been intensive research on the concentric-tube continuum robot, so called active cannulas or steerable needle for minimally invasive surgery (MIS) [1]~[7]. The most distinctive characteristic of this type of robot is that its distal end is steered and advances through rotation and translation of the pre-curved tubes relative to each other. Actuators are attached to the proximal ends of the tubes, and no other actuators are required such as pull-wires or pneumatic pumps [8], [9]. Therefore, the position of the robot's distal end and the robot's shape along it length can be controlled purely by rotating and translating the base of the tubes. This implicit actuating unit and the structural simplicity allow for small-scale design and give the robot great potential to be used as a new MIS instrument that incorporates the advantages of different types of conventional tools [10].

Energy stored in the concentric-tube continuum robot composed of multiple tubes usually has one minimum point, which determines the equilibrium conformations of the robot. Under some special condition, however, the robot can have more than one minimum energy point and thus have an unstable configuration in this kind of multi-stable state. Webster *et al*. called this phenomenon a "bifurcation" because the minimum point is separated in the energy landscape under certain condition [5]. Bifurcation should be avoided to ensure patient safety because it can cause the robot to suddenly move to another minimum energy point (called "Snapping") during operation. From a physical point of view, snapping occurs because of a burst of energy stored in the tubes. During relative rotational motion, the high bending stiffness and high curvature make the tube twist rather than bend, and the stacked energy makes the tube snap to a remote position. Therefore, either a control scheme needs to be specially designed, or the curvature of the tubes needs to be limited to avoid these configurations. Limiting the curvature of the tubes lowers the performance of the robot by limiting its workspace.

In this paper, we propose a new solution of making the tubes exhibit a lower bending stiffness to torsional stiffness ratio than normal isotropic tubes. This can be achieved by making grooves on the tube surface and reducing the bending stiffness more than the torsional stiffness. This method has been widely used for many medical instruments to improve their performances through both intuition and qualitative analysis. The most well-known example of a grooved tube is the guide wire inserted through a human vessel. Boston Scientific Corporation uses a microfabrication process that cuts minute slices in small-diameter nitinol tubes to improve the performance of a guide wire to access tortuous vasculature [11]. Haga *et al*. used femtosecond laser processing on a superelastic nitinol tube to fabricate a spring-shaped shape memory alloy (SMA) micro-coil with a square cross-section that bends easily [12]. Ryu *et al*. designed the flexible part of an SMA tube to have a series of slits with rounded ends to bend the needle preferentially in one direction under actuation [13].

There are several methods to process a cylindrical nitinol substrate. Most currently available stents are fabricated by laser cutting from nitinol tubing [14]. An alternative method to produce patterns with very thin struts is sputter deposition of nitinol [15]. The anisotropic material property can be generated by locally annealing nitinol micro-devices [16]. Electrochemical pulse etching is another method to fabricate complex microstructures from nitinol sheet [17]. In this paper, we adopted laser cutting to make grooves on superelastic nitinol tubes because it is appropriate for tubes at the robot's scale and ensures design flexibility [18].

*This research was supported by the National Research Foundation of Korea (NRF) (2012-041247), the Ministry of Science, ICT and Future Planning(2013K000371), and KIST Institutional Program (2E24132).

J. Kim and D. Lee are with the School of Mechanical and Aerospace Engineering, Seoul National University, Gwanak-ro, Gwanak-gu, Seoul 151-742, Korea (e-mail: rubagi05@gmail.com; winter2nf@gmail. com)

K. Kim and S. Kang are with the Center for Bionics, Korea Institute of Science and Technology, Hawolgok-dong, Wolsong-gil 5, Seongbuk-gu, Seoul, 136-791, Korea (e-mail: jazzpian@kist.re.kr; kasch804@gmail.com)

K. Cho is with the School of Mechanical and Aerospace Engineering, Seoul National University, Gwanak-ro, Gwanak-gu, Seoul 151-742, Korea (phone: +82-2-880-1663; fax: +82-2-880-1663; e-mail: kjcho@snu.ac.kr)

We verified the assumption that the tube anisotropy derived from the laser-cut surface grooves would alleviate or even eliminate the snapping problem in a concentric-tube continuum robot. The proposed method is a possible solution to the critical snapping problem in this type of robot. If the mechanical properties of the tubes can be modified as desired in further study, this method can offer some insights into the design of other tube-type medical devices.

II. Analysis

A. Review of Snapping Problem

Bifurcation occurs when the difference between the input angles of the overlapped tubes increases. Another local minimum appears separately in the energy landscape and becomes the global minimum as the present local minimum point disappears. The tube suddenly rotates to the new minimum energy point because of this phenomenon. This kind of movement is potentially dangerous, and avoiding bifurcation is a key parameters that should be considered in robot design.

To avoid this phenomenon, Dupont *et al*. [4] and Webster *et al*. [6] analyzed the conditions that generate bifurcation. Both research teams analyzed the "two tube case" and derived the same equation. Inequality (1) shows the condition to avoid this phenomenon. When the tube design satisfies (1), the robot will always have only one energy minimum point, which means that the robot can be stable for the whole work space.

$$L\sqrt{\kappa_1\kappa_2\frac{\frac{E_2I_2}{G_2J_2}+\frac{E_2I_2}{E_1I_1}\frac{E_1I_1}{G_1J_1}}{1+\frac{E_2I_2}{E_1I_1}}} < \frac{\pi}{2} \tag{1}$$

L is the length of the overlapped part, κ_1 and κ_2 are the curvatures of the two tubes, E is the elastic modulus, G is the shear modulus, and I and J are the area moment and polar moment of inertia, respectively. As shown in (1), the curvature and the overlapped length of the tube strongly affect the occurrence of bifurcation.

Having small values for the curvature and overlapped length would satisfy the above inequality and avoid bifurcation. However, limiting both values limits the workspace of the robot. The next target is the value of *EI/GJ*. Based on (1), *EI/GJ* has much more influence than the value E_2I_2/E_1I_1. To understand the meaning of the equation more intuitively, we assume that the inner and outer tubes have the same curvature and material properties, so (1) can be simplified as follows.

$$L\kappa\sqrt{\frac{EI}{GJ}} < \frac{\pi}{2} \tag{2}$$

Inequality (2) indicates that reducing *EI/GJ* can satisfy this condition and eliminate the bifurcation. Therefore, this term should be modified for the robot design if the overlapped length and curvature of the tubes are set as constant.

B. Tube Patterning Method

In a homogeneous isotropic linear elastic material, the following equation holds, where ν is Poisson's ratio.

$$E = 2(1+\nu)G \tag{3}$$

From the perpendicular axis theorem, equation (4) also holds.

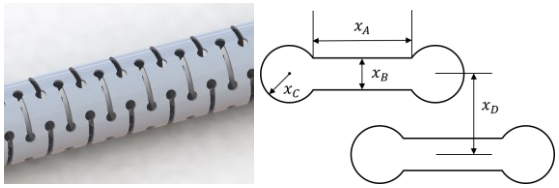

Figure 1. Shape of pattern and its design parameters.

$$2I = J \tag{4}$$

Therefore, in a homogeneous symmetrical material, *EI/GJ* is always equal to 1+ν. In other words, *EI/GJ* cannot be modified simply by changing the dimensions of the tube. The most feasible way to change *EI/GJ* is to cut certain patterns into the tube's surface. In this study, we induced anisotropic characteristics by making grooves on the tube via laser machining. Although the inherent material property cannot be changed on an infinitesimal scale, the specially designed pattern shown in Fig. 1 can make a tube anisotropic as a whole. The anisotropy occurs so that the bending stiffness is reduced by more than the torsional stiffness; this allows a robot to be designed with much fewer constraints while still satisfying (1) than a design using normal tubes.

To test the effects of the pattern, a simulation was performed using the simulation software ANSYS. Because the bending stiffness *EI* and torsional stiffness *GJ* of the grooved tube are impossible to calculate analytically, (5) and (6) were used to estimate *EI* and *GJ* [19]. These values were calculated by applying a force F or moment M, respectively, to the distal end of the tube and then measuring the displacement d, or rotation angle θ, respectively. l is the length of the tube specimen.

$$EI = \frac{Fl^3}{3\,d} \tag{5}$$

$$GJ = \frac{Ml}{\theta} \tag{6}$$

The outer and inner diameters of the simulated tube were 3.62 and 3.33 mm (the same sizes as the outer tube used in the actual experiment). Three patterns were placed on each circumference, and the center positions alternated line by line. Fig. 1 shows the shape of the pattern, and Table I shows the dimensions of the pattern used in the simulation. Vertically long pattern with the tube direction is likely to produce a weaker bending stiffness compared to torsional stiffness, and the ends of the pattern had a circular shape to reduce stress concentration. The pattern design was designed under two main considerations: (1) minimize *EI/GJ* of the processed tube,

TABLE I. Dimensions of Pattern Design

	x_A	x_B	x_C	x_D
Size	2 mm	0.25 mm	0.25 mm	1 mm

TABLE II. Simulation Results

	Bending Stiffness, *EI*	**Torsion Stiffness, *GJ***	***EI/GJ***
Normal Tube	180.7 mN · m²	133.3 mN · m²	1.35
Grooved Tube	5.9 mN · m²	14.9 mN · m²	0.40
Normal Tube /Grooved Tube	3.3%	11.2%	29.6%

and (2) reduce the stress concentration at both ends of the pattern under external loads. There was a tradeoff between these two requirements to some level, but an optimal design can be obtained by adjusting the shape and position of the pattern because it has many design parameters. This will be carried out in future work; in the present study, we used a representative pattern design as our focus was on whether this method can alleviate the snapping phenomenon.

The simulation result are summarized in Table II, where we compare the grooved tube with the normal tube. The simulation results showed that *EI/GJ* was reduced to 29.6% of its original value.

III. Fabrication

A Nd:YVO_4 laser system (wavelength of 355 nm, pulse duration of 30 ns, repetition rate of 100 kHz) was used to cut the pattern in the superelastic tubes. The maximum cutting depth of nitinol was about 150 μm with a maximum laser power of 2.6 W, scanner speed of 40 mm/s, and 40 repetition times. Therefore, the thickness of the tubes (supplied by Johnson Matthey Co Ltd.) was less than 150 μm. Although these tubes are thinner than those previously used for the tube continuum robots, the thickness of the tubes is irrelevant to the bifurcation phenomenon.

A. Tube Machining Process

The desired pattern spanned the tube's surface along the radial and axial directions. A particular system was required to cut the pattern into the curved surface with minimum distortion. Ideally, the rotation of the tube would be synchronized with the laser scanner movement to allow for continuous patterning, but this is technically demanding. To simplify the procedure, only one-sixth of the surface was processed at a time; the tube was then rotated 60° for further processing, and this was repeated for six times. As shown in Fig 2, a rotary motor stage (Unice E-O Service Inc., Taiwan) was used to precisely rotate the tube, a drill chuck fixed the tube, a cone-shaped bearing support prevented bending and twisting of the tube, and a linear guide fixed various tube lengths. A CCD camera (USB 2.0, Color 5MP CMOS camera, Mightex Systems, Pleasanton, CA, USA) was placed above the specimen to monitor dislocations of the tube after rotation, and an optoelectronic displacement measurement system (Micro-Epsilon, opto-NCDT 1402) was used to calibrate the tube's vertical position and focal length of the laser beam. Fig. 3 shows the laser-machined results.

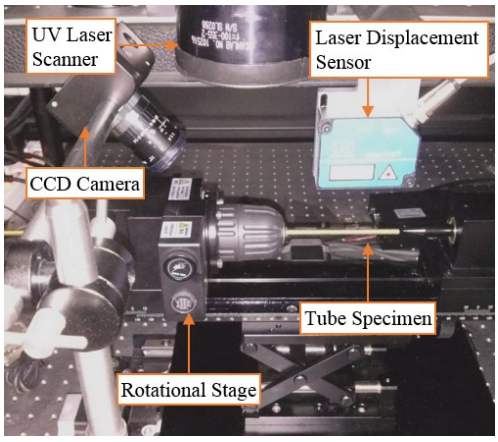

Figure 2. Laser machining setup for tube patterning.

Figure 3. Laser-machined tube specimen.

Figure 4. Annealed tubes and aluminum mold for annealing process.

B. Annealing Process

To curve the tubes, the normal tubes and grooved tubes were first placed in a box filled with dry ice. At this temperature, the tubes stayed in the martensite state, so they were much more compliant and easy to place in an aluminum mold. This mold was then placed in an air furnace at 520 ºC for 30 min followed by quenching in water. The annealing result and aluminum mold are shown in Fig. 4.

IV. Experimental Setup and Results

The tube properties were measured to verify that the ratio of the bending stiffness to the torsional stiffness had changed. After the change in stiffness ratio of the patterned tube was verified, both the inner and outer tubes were curved and rotated within one another to observe whether snapping occurred.

A. Measurement of material properties of tubes

Fig. 5 shows the experimental setups for measuring the bending stiffness and torsional stiffness. In the bending test, a tensile tester (R&B Micro lad RB302) was used; in the torsion test, a torque sensor (Transducer techniques TRT-50) and high-precision servo motor (Robotis H54-100) were used. A drill chuck was used to fix the tube specimens in both experiments.

Table III shows the dimensions of the tubes used in the experiments. There were some issues with measuring the normal tube specimen. Because the normal tube had high stiffness, it was likely to be crushed at the point where the load was applied during the bending test, and slip can occur

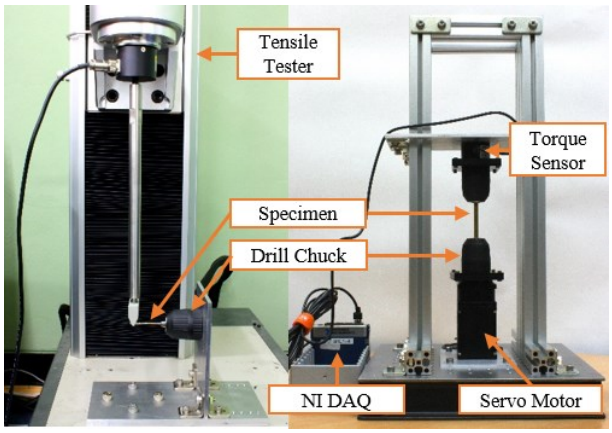

Figure 5. Experimental setup for tube property measurement: (left) bending test setup and (right) torsion test setup.

TABLE III. DIMENSIONS OF TUBES USED IN PROPERTY TEST

	Inner Dia.	Outer Dia.	Length
Bending Normal Tube	3.33 mm	3.62 mm	89.6 mm
Bending with Groove			40.7 mm
Torsion Normal Tube			30.0 mm
Torsion with Groove			38.2 mm

between the drill chuck and tube. To minimize the error caused by these issues, the tube specimen should be as long as possible. However, a longer tube makes it more difficult to align the tubes. Thus, we used a relatively long normal tube for the bending test and a shorter normal tube for the torsion test. In the torsion test, we prevented slip by using epoxy-based rough mounts at both ends of the specimen.

Figs. 6 and 7 show the experimental result. Because tubes with different lengths were used, the graph for the bending test (Fig. 6) plots $Fl^2/3$ versus y/l for intuitive comparison of the bending stiffness. The graph for the torsion test (Fig. 7) plots M versus θ/l for the same reason. Each experiment was conducted twice and produced almost the same results. The graph shows a dramatic reduction in the bending stiffness and torsional stiffness of the grooved tubes compared to the normal tubes. The results are summarized in Table IV. The bending stiffness and torsional stiffness were estimated by calculating the mean values of the slopes in the graphs.

EI/GJ was reduced from 1.49 to 0.57. The experimental results showed a discrepancy with the simulation results. We speculate that the crushing of the tube in the bending test and slipping of the tube in the torsion test may have caused this error. In addition, we set the Young's modulus of the material based on information provided by the manufacturer, but the actual values can be different. Even though the simulation could not accurately predict the result, the main idea that the pattern can reduce *EI/GJ* still holds.

B. *Tube rotation test*

To verify our concept, tube rotation tests were conducted. Two pre-curved tubes with different diameters were overlapped and rotated with respect to each other by 360°. For the normal tubes, snapping was observed. For the patterned tubes, the patterns interfered with each other and hindered the smooth translation or rotation. To solve this issue, a highly

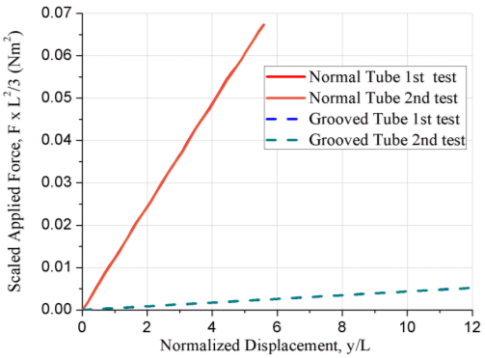

Figure 6. Results of the bending test. The graph plots $FL^2/3$ versus y/L, so the slope represents the bending stiffness.

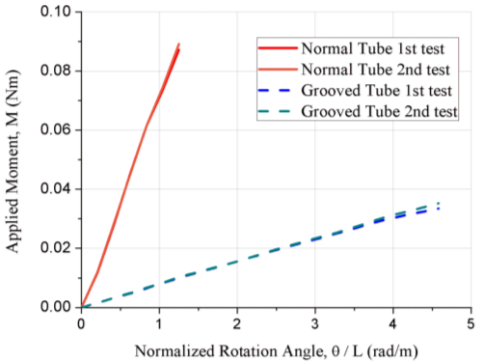

Figure 7. Results of torsion test. The graph plots M versus θ/l, so the slope represents the torsional stiffness.

TABLE IV. EXPERIMENTAL RESULT OF TUBE PROPERTY TEST

	Bending Stiffness, EI (Simulation)	Torsion Stiffness, GJ (Simulation)	EI/GJ (Simulation)
Normal Tube	109.4 mN · m² (180.7 mN · m²)	73.1 mN · m² (133.3 mN · m²)	1.49 (1.35)
Grooved Tube	4.2 mN · m² (5.9 mN · m²)	7.4 mN · m² (14.9 mN · m²)	0.57 (0.40)
Grooved tube /Normal tube	3.83% (3.3%)	10.1% (11.2%)	38.2% (29.6%)

abrasion-resistant polytetrafluoro ethylene (PTFE) tubing (supplied by Myungsung FEC Co Ltd., South Korea) was inserted between the inner and outer nitinol. Normal tubes with exactly the same dimensions and curvatures were prepared to compare the rotation result. Tables V and VI show the dimensions of the nitinol tubes and the PTFE tube between them, and Figs. 8 and 9 show the specimens used in the experiment.

TABLE V. DIMENSIONS OF TUBES USED IN TUBE ROTATION TEST

	Inner Tube	Middle Tube (PTFE)	Outer Tube
Outer Dia.	2.65 mm	3.00 mm	3.62 mm
Inner Dia.	2.35 mm	2.50 mm	3.33 mm

TABLE VI. GEOMETY OF TUBES USED IN EXPRIMENTS

	Radius of Curvature	Patterned Length (Only for patterned tube)	Curved Length	Straight Length
Inner Tube	40 mm	50 mm	50 mm	180 mm
Outer Tube	40 mm	50 mm	50 mm	100 mm

Figure 8. Normal (left) and grooved (right) tubes for tube rotation test. All four tubes had the same curvature.

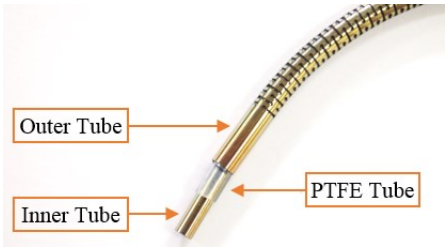

Figure 9. Assembled shape of grooved tube with PTFE tube. The PTFE tube was used to reduce the inter-locking between the inner and outer grooved tubes.

The experimental setup in Fig. 10 was used to generate relative rotational motion of the tubes. Collet chucks were used to grip the tubes, and motors (Maxon Motors, RE25, 20 W) were used to rotate the tubes. In the experiment, two tubes were fully overlapped; one tube was fixed, and the other tube was rotated. The movement of the distal end of the continuum robot was recorded by a video camera, and the trace data of the distal end was acquired using visual analysis software (Xcitex, ProAnalyst).

Fig. 11 shows the visual tracking results. The green and red marks show the traced distal ends of the normal and grooved tubes, respectively. The left figure shows the trace of the normal tubes, and the right figure shows the trace of the grooved tubes. The left figure shows a snapping point that remains blank in the trace, while the right figure shows a continuous trace of the red line, which means that snapping did not occur. The trace data were rearranged and plotted by setting the input angle to 0 º when the curve directions of the two tubes were aligned with each other. Fig. 12 shows that the snapping occurred in normal tubes at around 180 º of the input angle, and the tubes suddenly rotated by 20 º at that point. These results indicate that the snapping phenomenon can be prevented by using the grooved tubes with anisotropic properties.

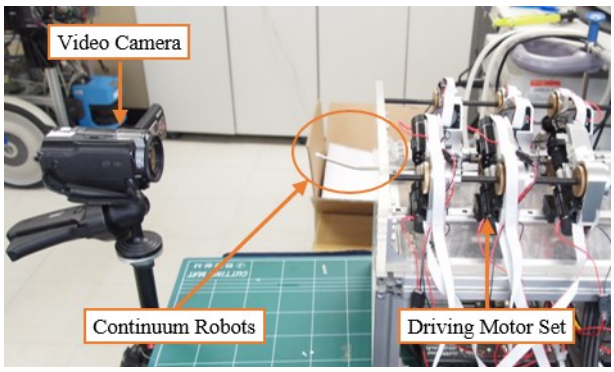

Figure 10. Experimental setup for tube rotation test. Snapping movement was observed by visual analysis.

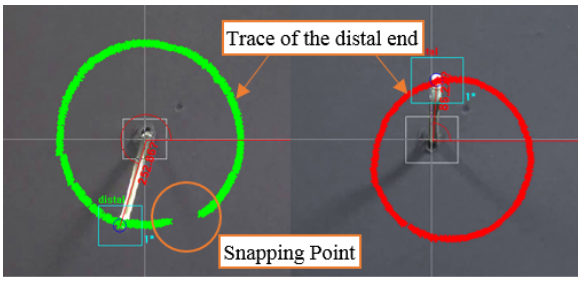

Figure 11. Video analysis of distal tracking. Green marks (left) show the traced distal end of the normal tubes, and red marks (right) show the traced distal end of the grooved tube. The left figure shows the snapping movement.

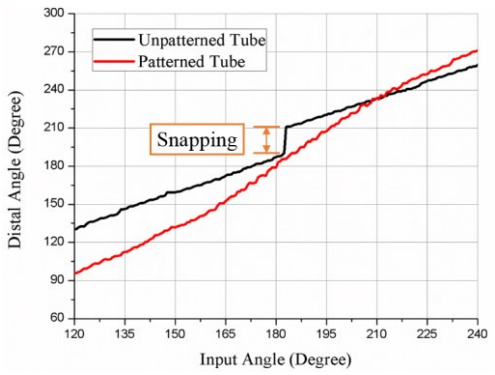

Figure 12. Resultant graph of video analysis. The normal tubes showed snapping at an input angle of around 180°. The snapping angle was about 20°.

V. Discussion

When applying the concept of using grooved nitinol tubes for the concentric-tube continuum robot, the foremost issue was moving the processed tubes relative to each other. Because the tubes are grooved, curved, and overlapped, the grooves seriously hinder the relative translational and rotational motions of both tubes. Sometimes the tubes become interlocked and completely stuck together, which makes it almost impossible to make further movements without breaking them. Therefore, the PTFE tube between the two tubes is an essential structural component in our concept. However, the additional tubing inevitably makes the whole structure bulkier, and the PTFE tube starts to become abraded after a few repeated operations. This problem can be solved by using two ultra-thin heat shrink PTFE tubing: one on the outer surface of the inner tube and the other on the inner surface of the outer tube.

The next issue was the dramatic variation in mechanical properties of the tubes. As shown in the simulation and experimental result, the grooved tube had much less stiffness compared to the normal tube, which can be a drawback of this method. However, the reduction ratio can be controlled by pattern design, and also the grooved region can be resized based on specific requirements. Moreover, this characteristic can be a method to build a dominating stiffness tube pair, which is one of the control scheme of the tube continuum robot [1]. For practical application, this characteristic need to be studied in all its aspects.

Finally, the grooved patterns should be optimized to determine the most desirable combination of decreased *EI/GJ* and decreased stress concentration under external loads. The pattern has four design parameters, and the pattern shape or parameters can be changed to determine the optimal design for specific tube dimensions. In this way, the snapping problem can be overcome while maintaining the robot's steering ability without compromising its workspace.

VI. Conclusion

We demonstrated that making certain groove patterns on superelastic nitinol tubes can be one solution to the snapping problem in concentric-tube continuum robots. Two sets of tubes with the same specifications, where one set was patterned and the other was not, showed different behavior under continuous rotation: the normal tubes snapped, while the grooved ones did not. Although the feasibility of our method was demonstrated, some issues remain regarding the interlocking, and pattern optimization. In addition, the effect of large variations for the stiffness of the tube should be analyzed carefully. Provided that these issues are resolved, our approach can be implemented in the design of the concentric-tube continuum robots to allow for more freedom in the workspace and trajectory. This approach may also be used for other cylindrical medical devices.

Acknowledgment

The authors thank Kwang-Koo Jee for the annealing process of nitinol tubes and Tae-Young Choi for experimental support.

References

[1] S. Patrick and P. Dupont. "A steerable needle technology using curved concentric tubes." *Intelligent Robots and Systems (IROS), IEEE/RSJ International Conference on*, pp. 2850-2856, 2006.

[2] R. J. Webster III, A. M. Okamura, and N. J. Cowan. "Toward active cannulas: Miniature snake-like surgical robots." *Intelligent Robots and Systems (IROS), IEEE/RSJ International Conference on*, pp. 2857-2863, 2006.

[3] D. C. Rucker and R. J. Webster, "Parsimonious evaluation of concentric-tube continuum robot equilibrium conformation," *Biomedical Engineering, IEEE Transactions on*, vol. 56, no. 9, pp. 2308-2311, 2009.

[4] P. Dupont, J. Lock, E. Butler, "Torsional Kinematic Model for Concentric Tube Robots," *Robotics and Automation (ICRA), IEEE International Conference on*, pp. 3851-3858, 2009.

[5] R. J. Webster, J. M. Romano and N. J. Cowan, "Mechanics of precurved-tube continuum robots," *Robotics, IEEE Transactions on*, vol. 25, no. 1, pp. 67-78, 2009.

[6] D. C. Rucker, R. J. Webster, G. S. Chirikjian and N. J. Cowan, "Equilibrium conformations of concentric-tube continuum robots," *The International Journal of Robotics Research*, vol. 29, no. 10, pp. 1263-1280, 2010

[7] P. E. Dupont, J. Lock, B. Itkowitz and E. Butler, "Design and Control of Concentric-Tube Robots," *Robotics, IEEE Transactions on*, vol. 26, no. 2, pp. 209-225, 2010.

[8] Y. Fu, H. Liu, W. Huang, S. Wang and Z. Liang, "Steerable catheters in minimally invasive vascular surgery," *The International Journal of Medical Robotics and Computer Assisted Surgery*, vol. 5, no. 4, pp. 381-391, 2009.

[9] K. Ikuta, H. Ichikawa, K. Suzuki and D. Yajima, "Multi-degree of freedom hydraulic pressure driven safety active catheter," *Robotics and Automation (ICRA), 2006 IEEE International Conference on*, pp. 4161-4166, 2006.

[10] N. V. Vasilyev, A. H. Gosline, E. Butler, N. Lang, P.J. Codd, H. Yamauchi, E. N. Feins, C. R. Folk, A. L. Cohen, R. Chen, D. Zurakowski, P. J. Nido P. E. Dupont, "Percutaneous Steerable Robotic Tool Delivery Platform and Metal Microelectromechanical Systems Device for Tissue Manipulation and Approximation Closure of Patent Foramen Ovale in an Animal Model," *Circulation: Cardiovascular Interventions*, 6(4), pp. 468-475, 2013.

[11] http://www.bostonscientific.com/peripheral-interventions/products.html#productDetailPage(10138011)

[12] Y. Haga, Y. Muyari, S. Goto, T. Matsunaga and M. Esashi, "Development of Minimally Invasive Medical Tools Using Laser Processing on Cylindrical Substrates," *Electrical Engineering in Japan*, vol. 176, no. 1, pp. 65-74, 2011.

[13] S. C. Ryu, P. Renaud, R. J. Black, B. L. Daniel and M. R. Cutkosky, "Feasibility study of an optically actuated MR-compatible active needle," *Intelligent Robots and Systems (IROS), 2011 IEEE/RSJ International Conference on*, pp. 2564-2569, 2011.

[14] T. Duerig, D. Stoeckel and D. Johnson, "SMA: smart materials for medical applications," *European Workshop on Smart Structure in Engineering and Technology*, International Society for Optics and Photonics, pp. 7-15, 2003.

[15] V. Gupta, V. Martynov and A. D. Johnson, "Recent developments in SMA thin film based microactuators for biomedical and fiber optics applications," *Actuator*, vol. 2002, pp. 355-358, 2002.

[16] Y. Bellouard, T. Lehnert, J. E. Bidaux, T. Sidler, R. Clavel and R. Gotthardt, "Local annealing of complex mechanical devices: a new approach for developing monolithic micro-devices," *Materials Science and Engineering: A 273*, pp. 795-798, 1999.

[17] T. Mineta, T. Mitsui, Y. Watanabe, S. Kobayashi, Y. Haga and M. Esashi, "Batch fabricated flat meandering shape memory alloy actuator for active catheter," *Sensors and Actuators A: Physical*, vol. 88, no. 2, pp. 112-120, 2001.

[18] A. T. Tung, B. H. Byung, G. Niemeyer and D. H. Liang, "Laser-machined shape memory alloy actuators for active catheters," *Mechatronics, IEEE/ASME Transactions on*, vol. 12, no. 4, pp. 439-446, 2007.

[19] E. P. Popov, *Engineering Mechanics of Solids*, PHI Learning, 2009.